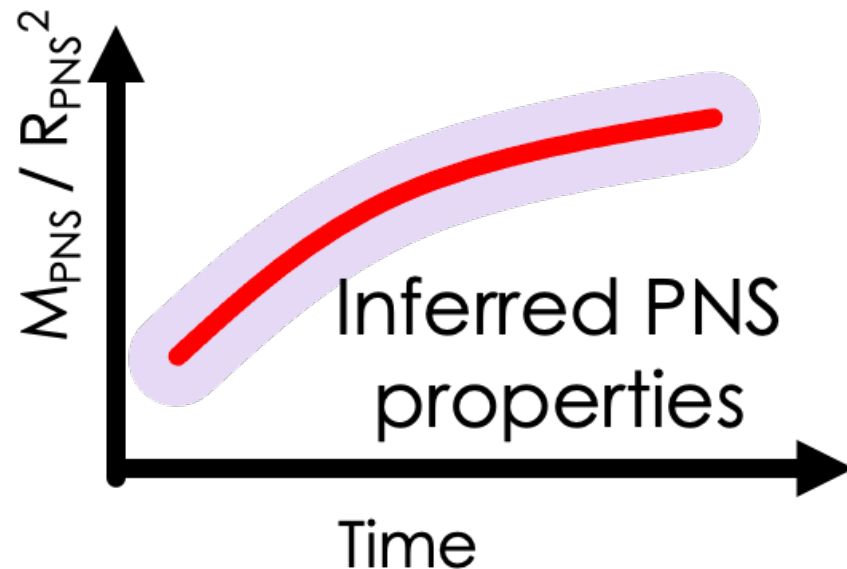


# Inference with CCSN waveforms



José Antonio Font  
Universitat de València  
[www.uv.es/virgogroup](http://www.uv.es/virgogroup)



# Outline

- ❑ Introduction
- ❑ Asteroseismology of PNS
- ❑ Quasi-universal relations
- ❑ Inference of CCSN - our method
- ❑ Observational constraints for neutrino-driven CCSN
- ❑ The case of rapidly-rotating CCSN

Talk based on:

Bizouard et al, PRD, 103, 063006 (2021)

Torres-Forné et al, PRL, 123, 051102 (2019)

Torres-Forné et al, MNRAS, 482, 3967 (2019); 474, 5272 (2018)

Bruel et al, in preparation (2021)

Pastor-Marcos et al, in preparation (2021)

Talk is a continuation of Pablo Cerdá-Duran's presentation at WS1

<https://www.youtube.com/watch?v=WuKQCg9YJCk>



# Introduction

**Core-Collapse Supernovae (CCSN)** are a prime source of gravitational waves.

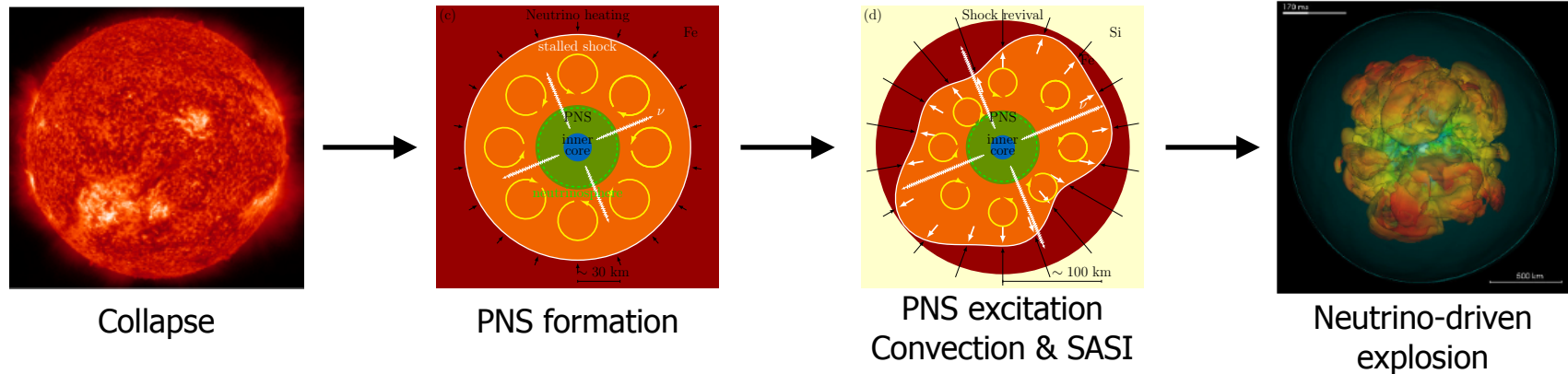
Their typical frequencies make them perfect targets for ground-based detectors.

A successful detection could potentially:

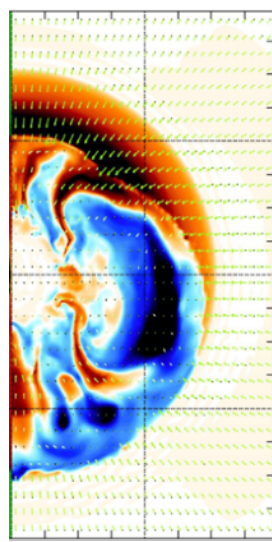
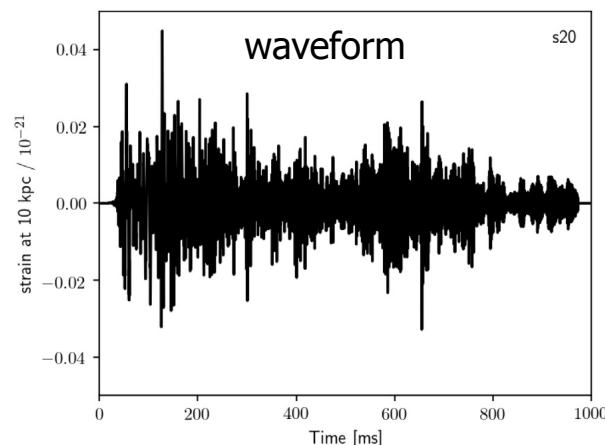
- Reveal underlying **explosion mechanism** through analysis of the waveform.
- Reveal properties of progenitor and/or new-born (**proto-**) **neutron star (PNS)**.

## CCSN progenitors:

- massive stars 8-100 Msun
- Non-rotating (>99%)  
[\(Li+ 2011, Chapman+ 2007\)](#)
- Observable within  $\sim 10$  kpc  
[\(Gossan+ 2015, Powell & Müller 2018\)](#)
- Rare events: 1/30 yr in our Galaxy [\(Adams+ 2013\)](#)



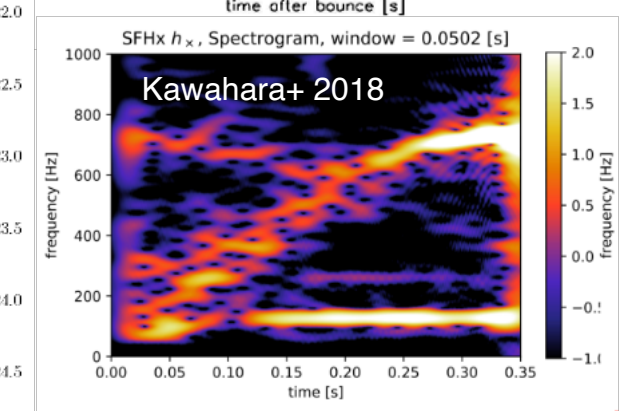
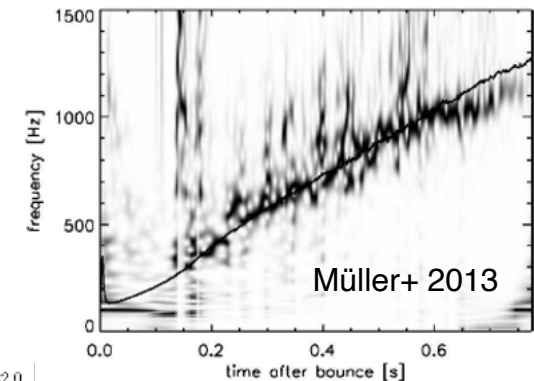
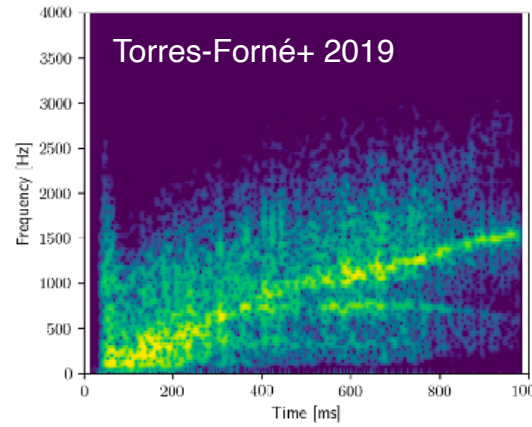
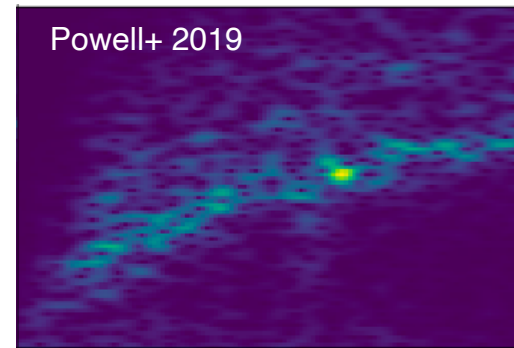
# Gravitational waves from PNS oscillations



Numerical simulation  
(Obergaulinger+ 2013)

- Highly stochastic GW signal
- Frequencies evolve with time (g-modes, SASI)

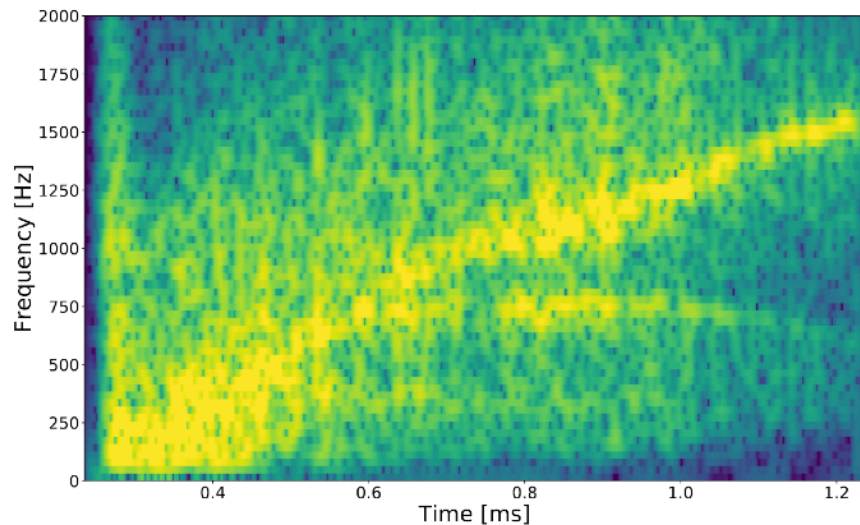
spectrograms



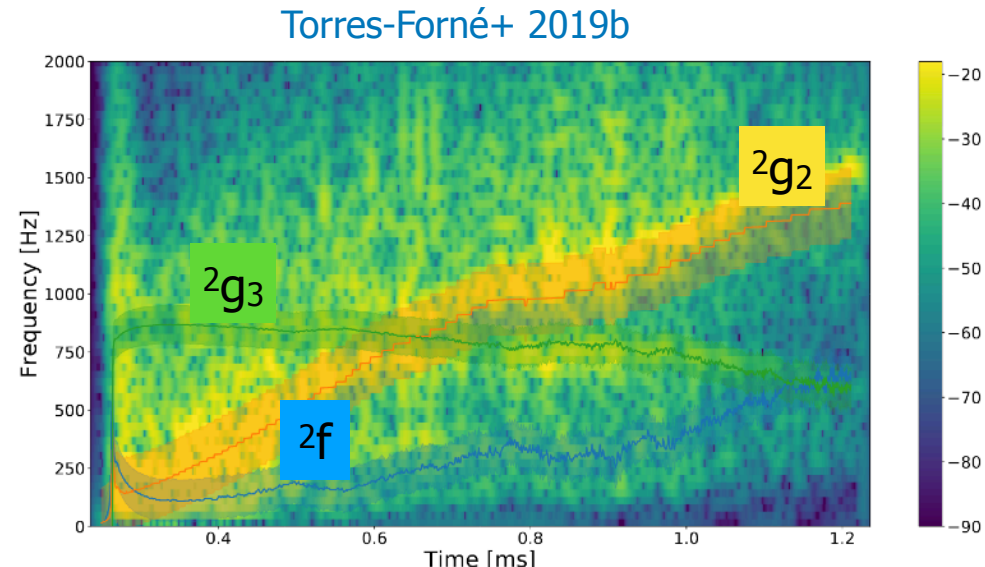
arch-shaped features observed by different groups (multiple codes)



# Gravitational waves from PNS oscillations



GW spectrogram from a  $20M_{\odot}$  progenitor (Cerdá-Durán+ 2013)



Features in spectrograms can be matched to specific PNS eigenmodes.

- **p-modes** and **f-mode**.

Fundamental p-mode.

$$L^2 \approx c_s^2 \frac{l(l+1)}{r^2}$$

Restoring force is pressure.  $f \propto c_s \propto \sqrt{\rho} \propto \sqrt{\frac{M}{R^3}}$

- **g-modes**

Gravity modes.

Restoring force is buoyancy.

$$N^2 \approx \frac{\partial \Phi}{\partial r} \frac{1}{\rho} \left( \frac{1}{c_s^2} \frac{\partial P}{\partial r} - \frac{\partial \rho}{\partial r} \right)$$

$$f \propto \frac{M}{R^2} \times \sqrt{\frac{(\Gamma - 1)m_n}{\Gamma k_b T}}$$

- Which one is the dominant mode?
- How does it depend on PNS properties?



PNS asteroseismology

# Quasi-universal relations

Through numerical simulations of CCSN we show that the characteristic frequency for the different PNS modes does not depend on the exact structure of the PNS but can be estimated from the general properties of the remnant.

The **time-frequency relations (fits)** are **quasi-universal**, as they do not depend on the EoS, progenitor star, or neutrino treatment.

Those relations provide the potential to be used for parameter inference once actual GW observations from CCSN become available.

- 25 1D simulations
- 2 codes: AENUS-ALCAR ([Obergaulinger 2008; Just+ 2015](#)) & CoCoNuT ([Dimmelmeier+ 2005](#))
- 6 EoS: LS220, Gshen-NL3, Hshen, SFHo, BHB- $\Lambda$ , Hshen- $\Lambda$
- 8 progenitors: 11.2 - 75 M<sub>sun</sub>

- fits  $f = a + bx + cx^2 + dx^3$

$$x = \sqrt{\frac{M_{\text{shock}}}{R_{\text{shock}}^3}}$$

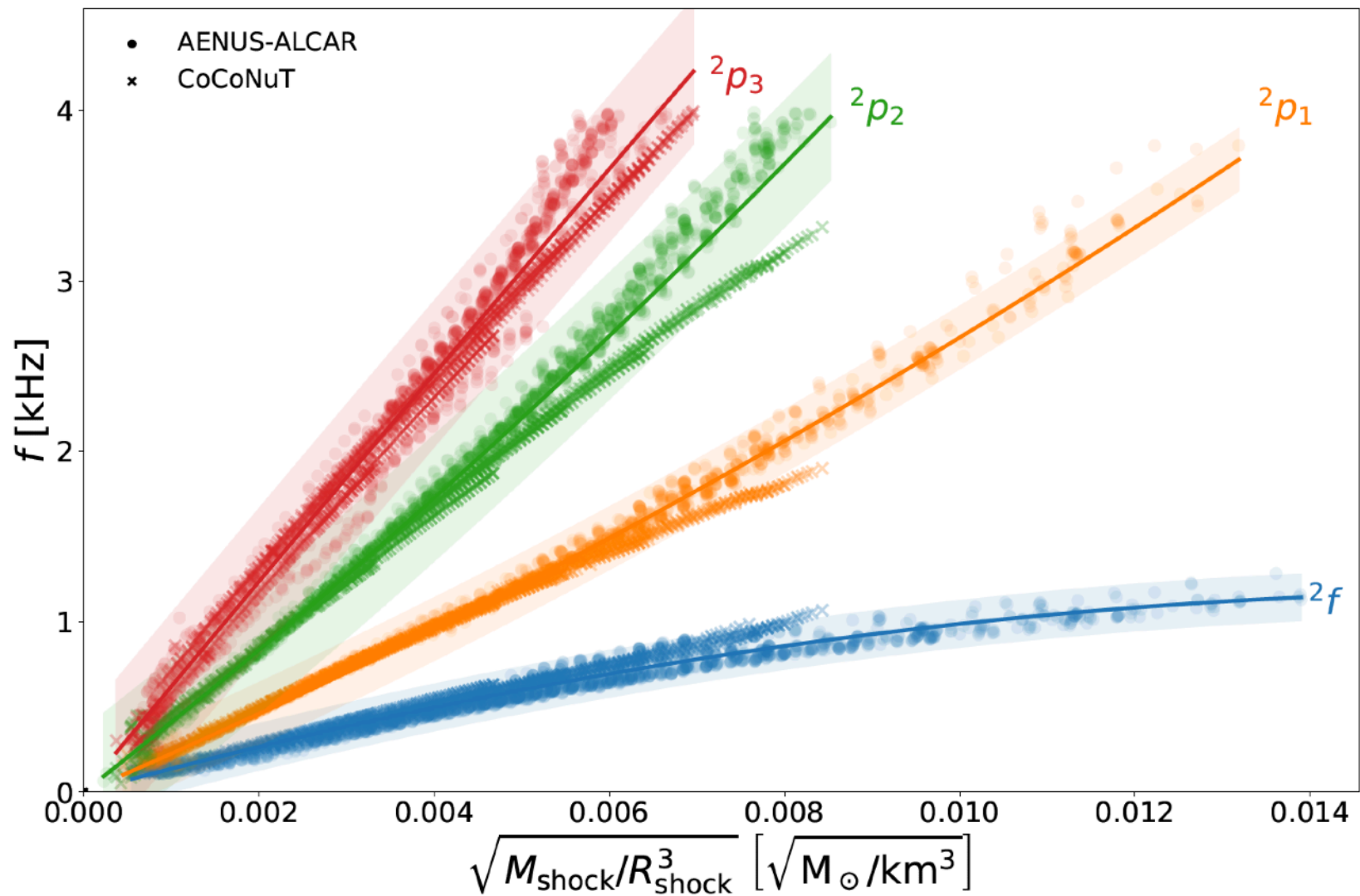
f-mode and p-modes

$$x = \frac{M_{\text{PNS}}}{R_{\text{PNS}}^2}$$

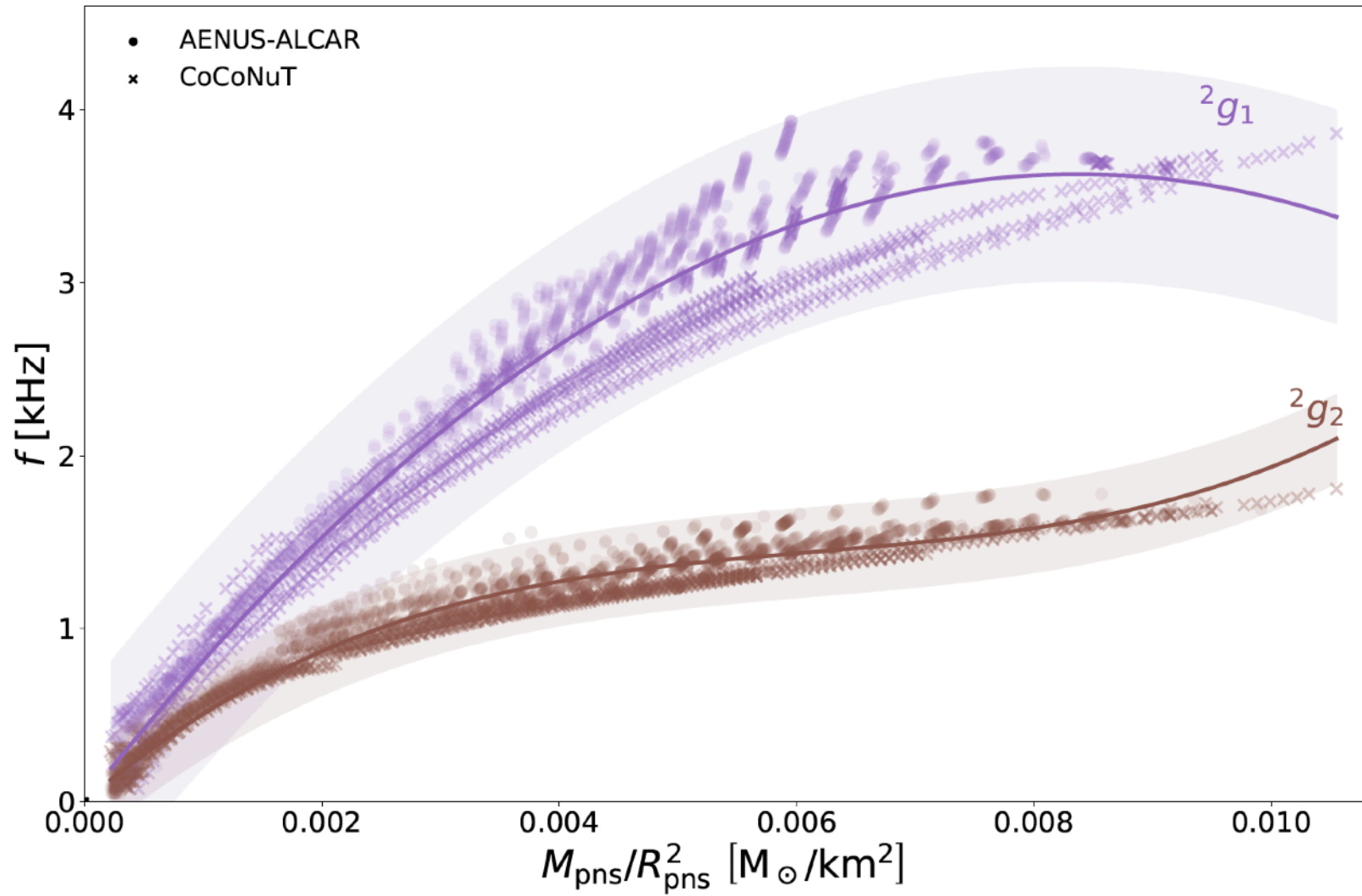
g-modes



# Quasi-universal relations



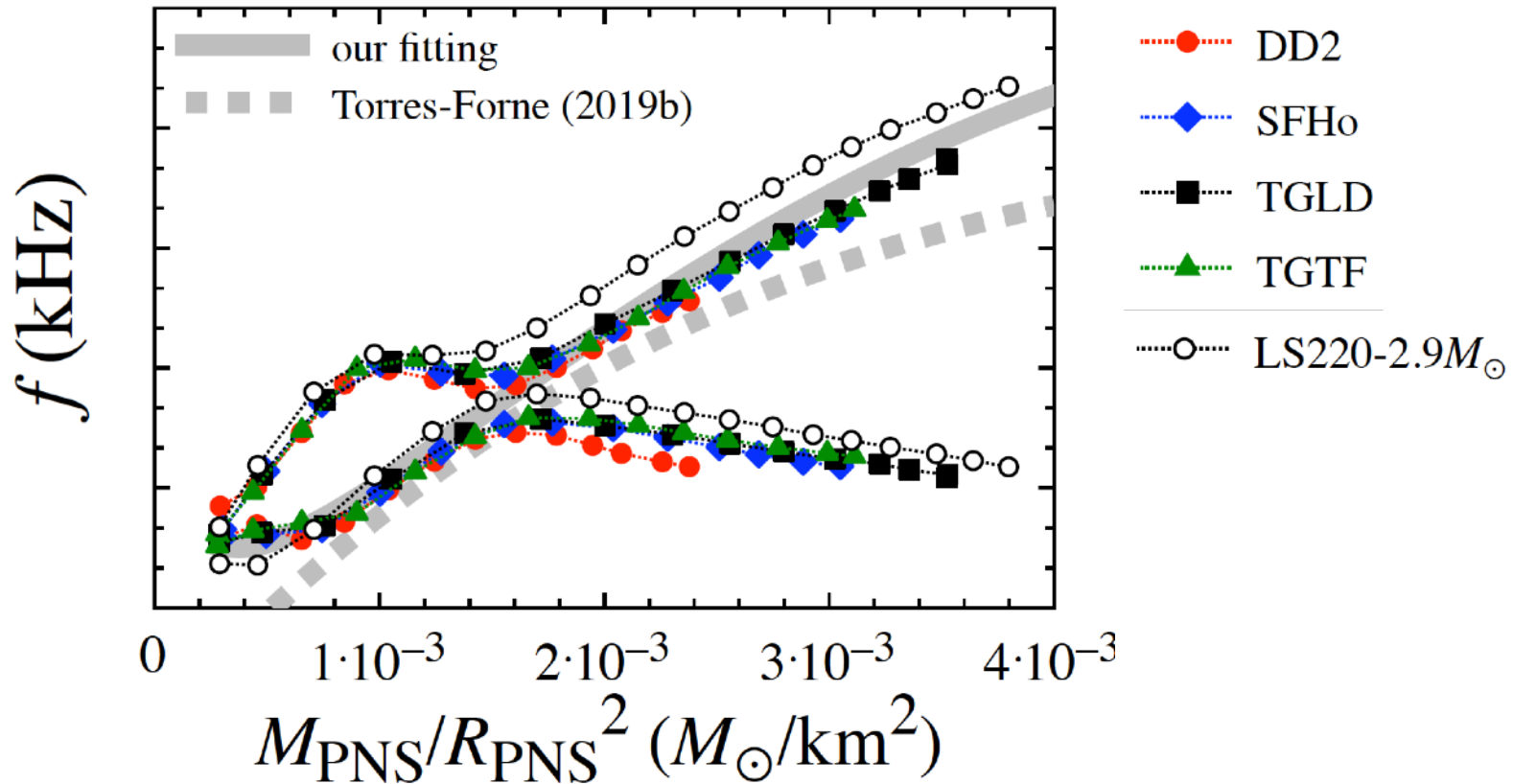
# Quasi-universal relations



# Quasi-universal relations - 2D models by H. Sotani

2D radiation hydrodynamics CCSN simulations with 3DnSNe code  
(Takiwaki+ 2016, Kotake+ 2018)

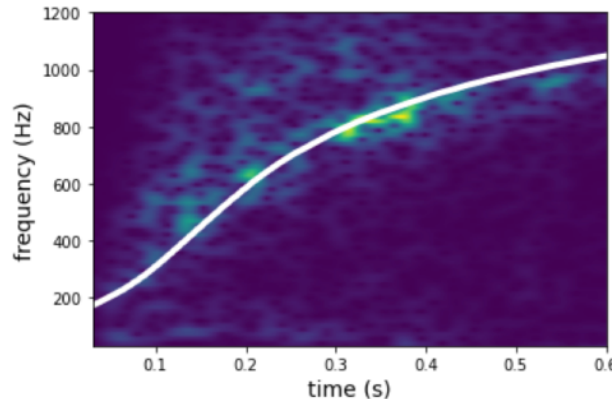
20M<sub>sun</sub> progenitor of Woosley & Heger (2007)



Sotani+ 2021



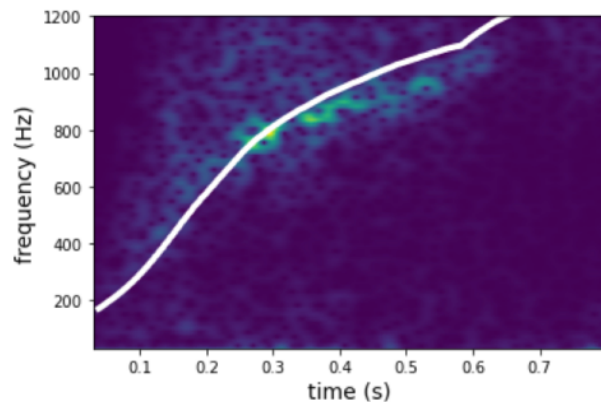
# Quasi-universal relations - 3D models by J. Powell



$^2g_2$  mode evolution

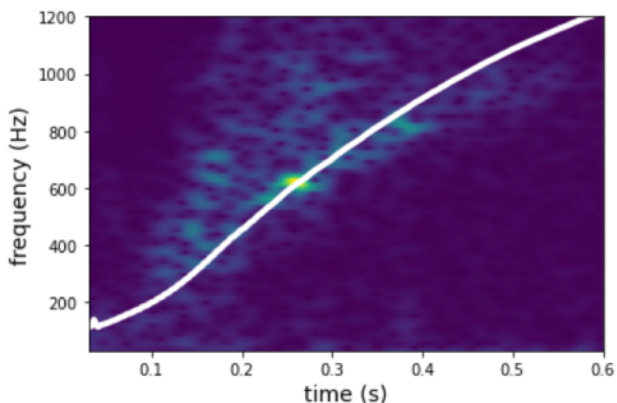
## Model He3.5 (Powell & Müller 2018)

Ultra-stripped star evolved from a helium star with an initial mass of  $3.5 M_{\text{sun}}$  (Tauris+ 2015)



## Model s18 (Powell & Müller 2018)

Solar metallicity progenitor star with a ZAMS mass of  $18 M_{\text{sun}}$ .



## Model y20 (Powell & Müller 2020)

$20 M_{\text{sun}}$ , non-rotating, solar metallicity helium (Wolf-Rayet) star from Yoon (2017)

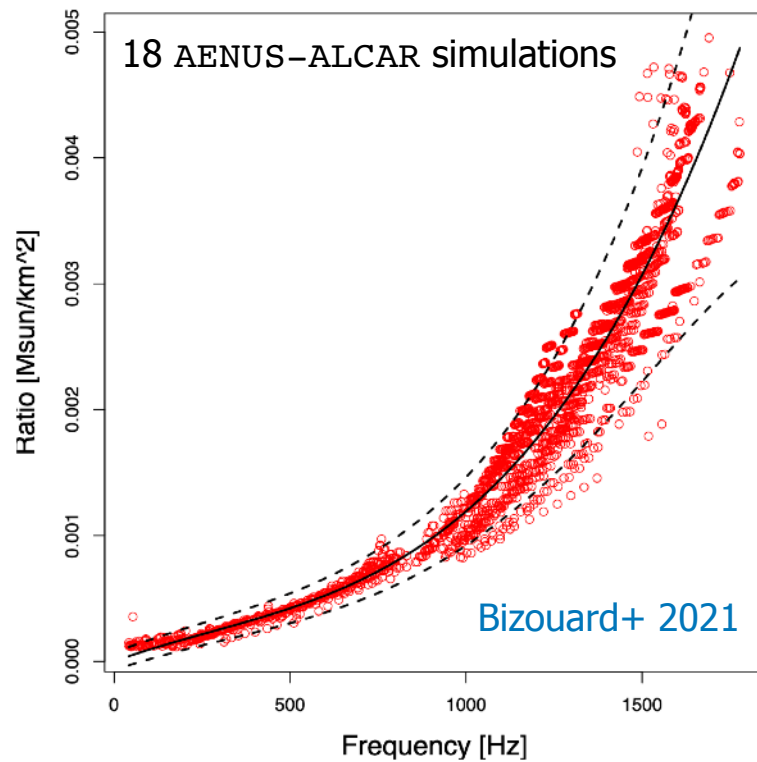


# Inference: method

We focus on the  $^2g_2$  mode (main feature in spectrograms)

**Goal:** measure the time evolution of the ratio  $r = \frac{M_{\text{PNS}}}{R_{\text{PNS}}^2}$  in GW data.

**Step 1 of the method:** Build a model that relates the ratio to the frequency evolution of the GW signal,  $r(f)$ , using 1D simulations (model set) and quasi-universal relations.



Discretized ratio parametrized with cubic polynomial regression with heteroscedastic errors

$$r_i = \beta_1 f_i + \beta_2 f_i^2 + \beta_3 f_i^3 + \epsilon_i$$

Errors take into account dispersion at high frequency. Zero-mean Gaussian error with variance  $\sigma_i$

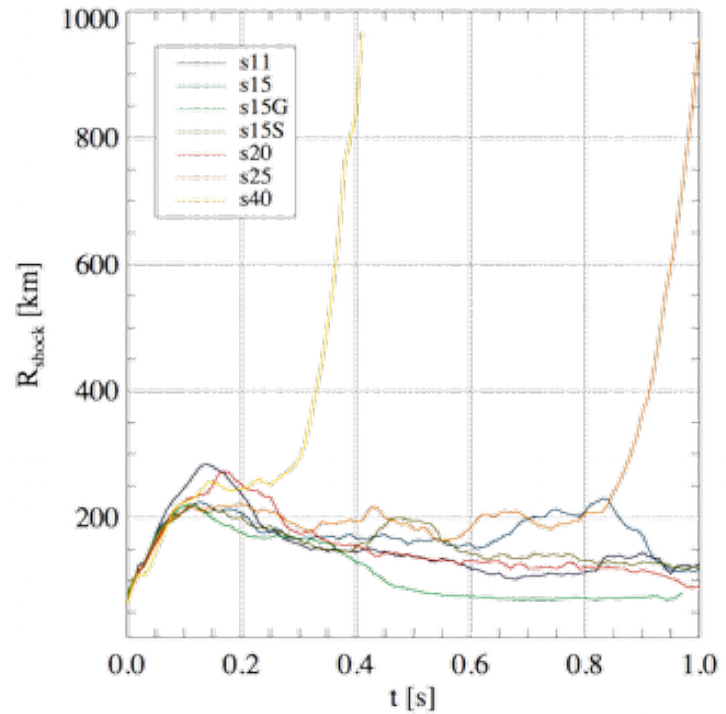
$$\log \sigma_i = \alpha_0 + \alpha_1 f_i + \alpha_2 f_i^2 + \delta_i$$

R-package `lmvar` to fit the model using maximum likelihood approach.

# Inference: method

**Step 2 of the method:** Use 2D simulations (test set) for which  $r(t)$  is known to validate model and provide detectability estimates.

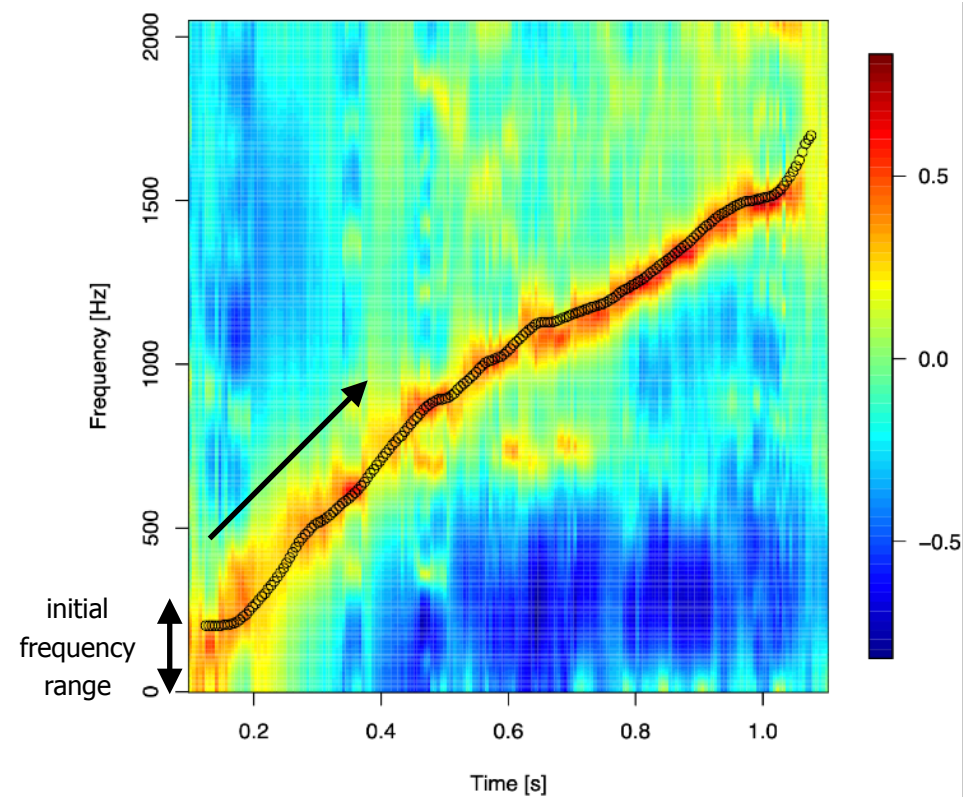
Model name	$M_{\text{ZAMS}}$ [ $M_{\odot}$ ]	progenitor model	EOS	$t_f$ [s]	$t_{\text{explosion}}$	$M_{\text{PNS,f}}$ [ $M_{\odot}$ ]
s11	11.2	[50]	LS220	1.86	×	1.47
s15	15.0	[50]	LS220	1.66	×	2.00
s15S	15.0	[50]	SFHo	1.75	×	2.02
s15G	15.0	[50]	GShen	0.97	×	1.86
s20	20.0	[50]	LS220	1.53	×	1.75
s20S	20.0	[51]	SFHo	0.87	×	2.05
s25	25.0	[50]	LS220	1.60	0.91	2.33
s40	40.0	[50]	LS220	1.70	1.52	2.23



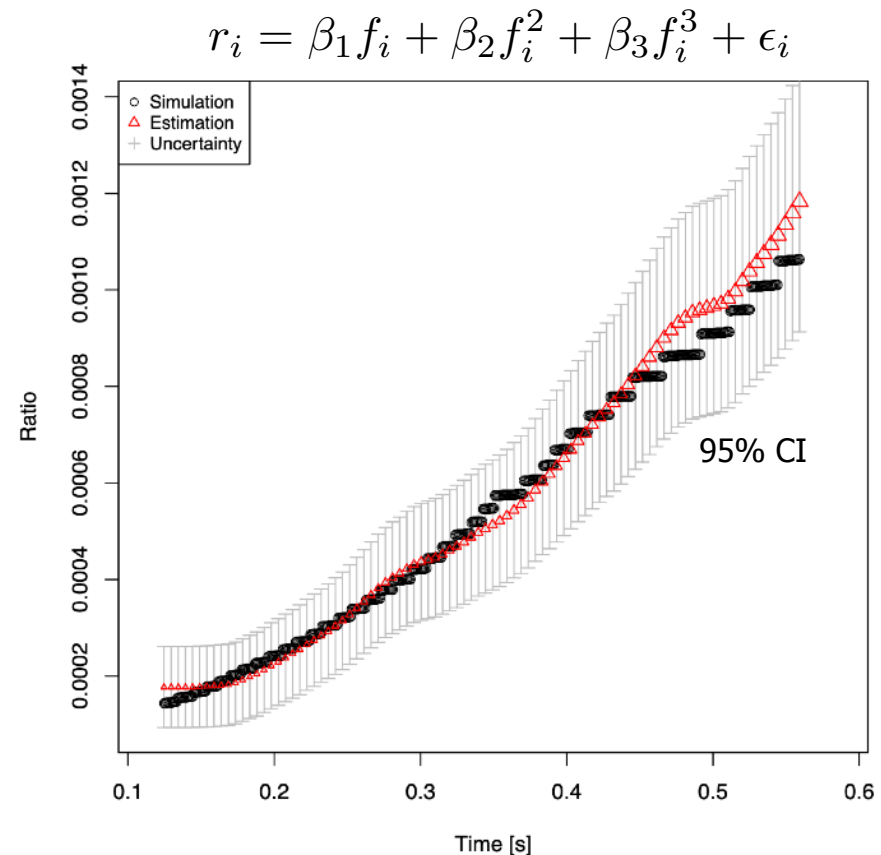
# Inference: method

We compute the spectrogram and search for the  $^2g_2$  mode frequency track (peak frequency using a simple track-finding algorithm)

- Starting frequency range: [0, 200] Hz
- Mode frequency can only grow



Example with s20S GW signal



Bizouard+ 2021



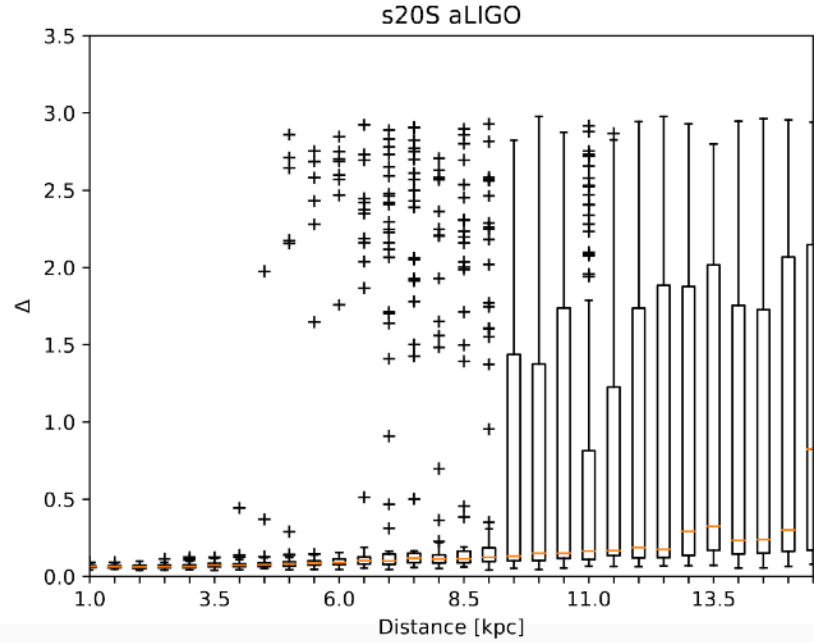
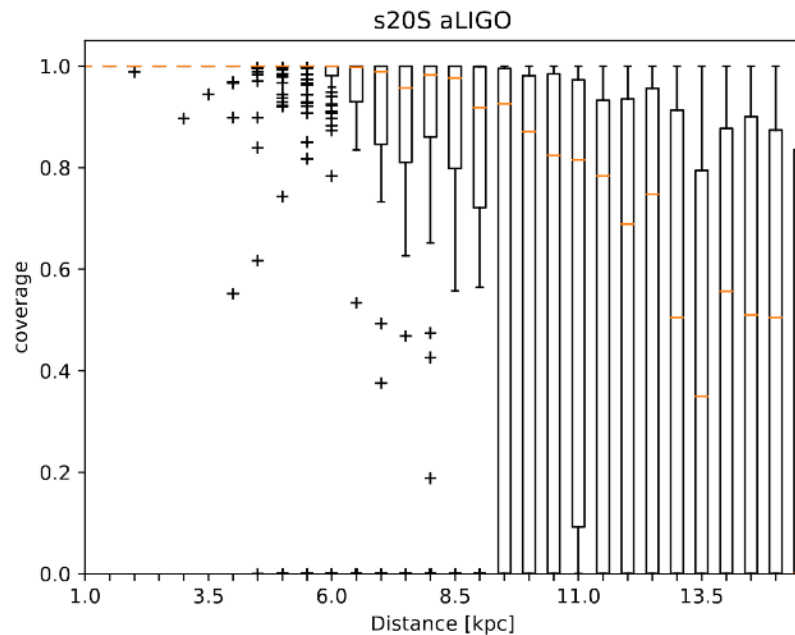
# Detectability prospects: s20S waveform

Inject s20S GW signal into 100 Gaussian noise realizations (design Advanced LIGO PSD)

- Source optimally oriented wrt detector
- Assume CCSN GW signal has been identified in the data

Vary distance and compare reconstructed ratio to true ratio, using coverage (fraction of values within 95% CI) and relative error  $\Delta$

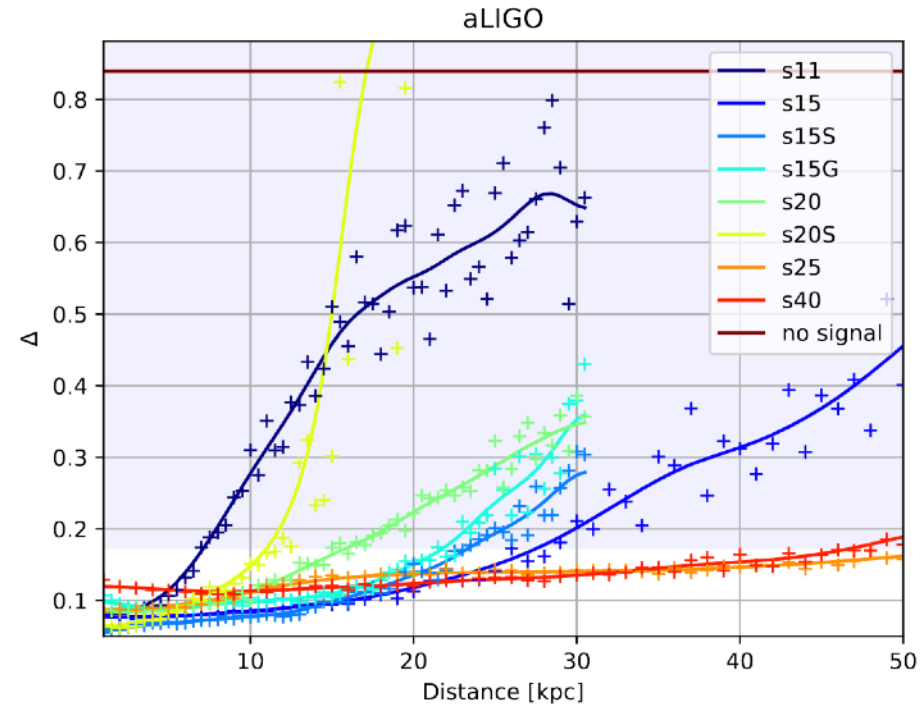
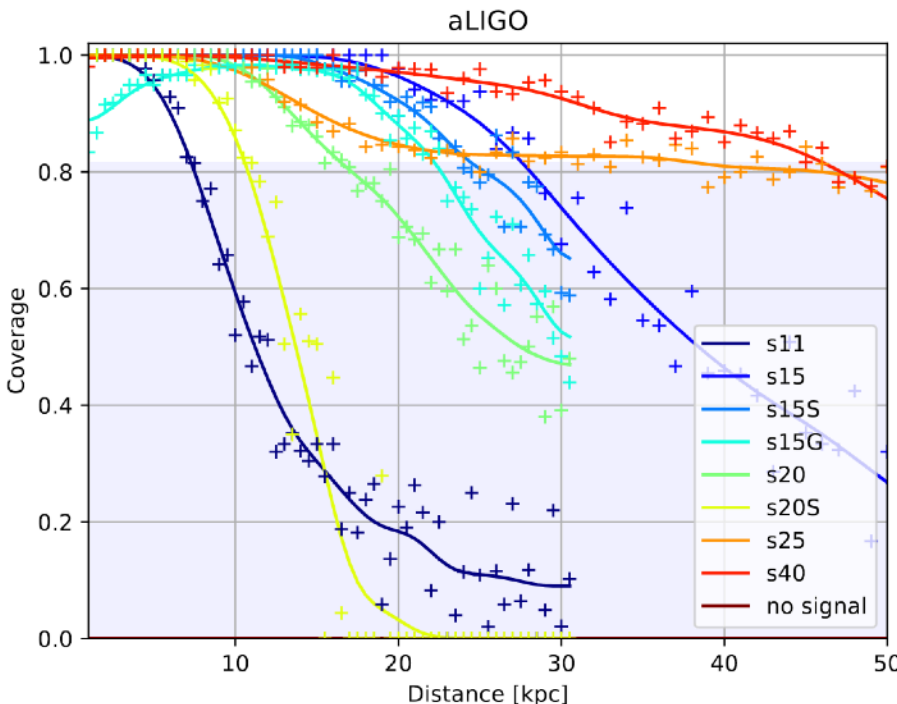
$$\Delta = \frac{1}{N} \sum_1^N \frac{|r_i - r_i^0|}{r_i^0}$$



# Detectability prospects: all waveforms

Test that the method does not depend on the waveform.

Performance: distance at which ratio can be reconstructed with a coverage < 95 % of the noise-only coverage values.



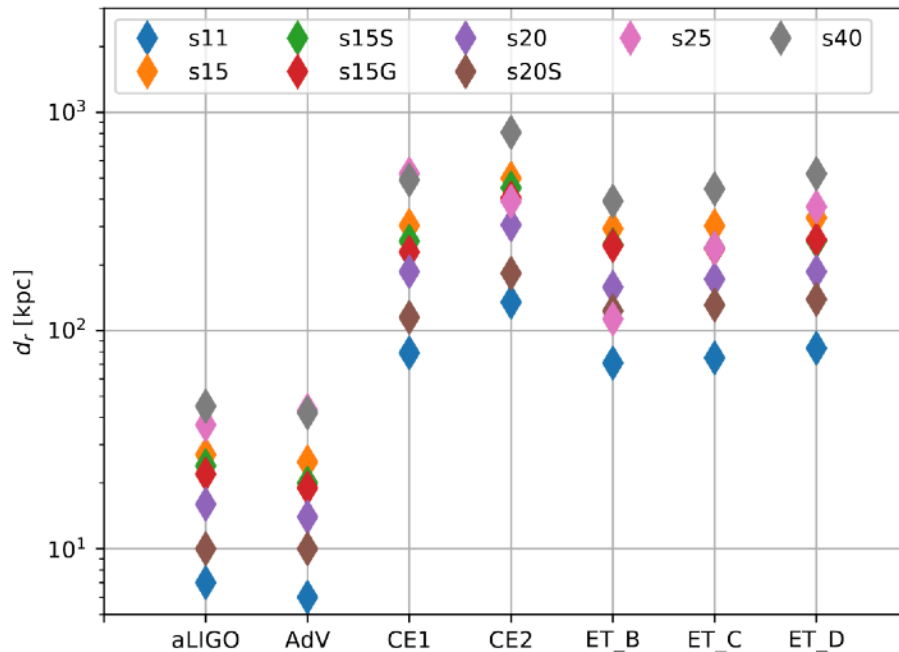
Ratio well reconstructed for all waveforms (except s11 AND s20S) up to  $\sim 15$  kpc.

Coverage > 80% and Error < 20%

# Detectability prospects: 2G and 3G detectors

**Maximal distance** at which the ratio  $r = \frac{M_{\text{PNS}}}{R_{\text{PNS}}^2}$  is reconstructed with good accuracy for 2G and 3G detectors.

[Good accuracy = median of coverage < 95% of noise-only values]



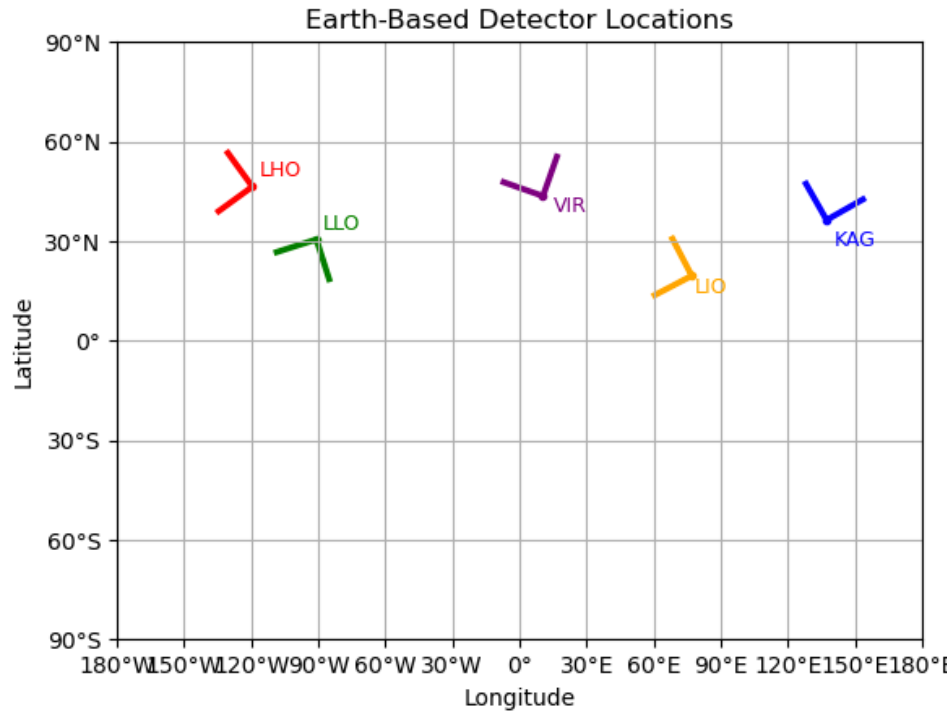
Bizouard+ 2021

Cosmic Explorer and Einstein Telescope: [CE1, CE2: [Reitze+ 2019](#); ET\_B, ET\_C, ET\_D: [Hild+ 2011](#)]

- Ratio reconstructed up to distance 100-700 kpc.
- Best sensitivity above few hundred Hz most important parameter (low frequency <10 Hz sensitivity does not matter)

# Multi-detector coherent analysis

Motivation: more realistic working case taking into account the sky position of the source and the location/orientation of each ground-based detector ([Bruel+ 2021](#))



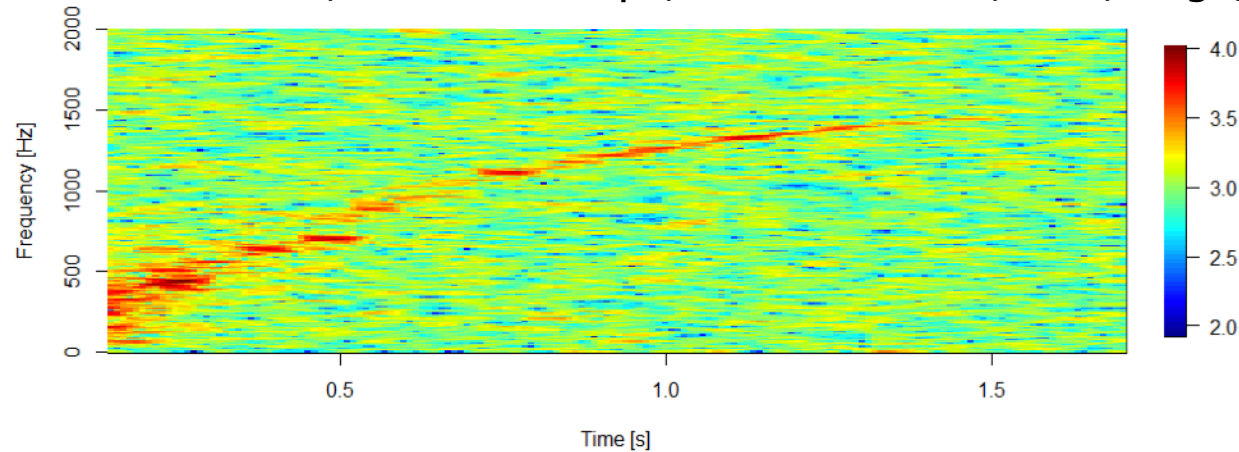
Network of 5 2G detectors (LHO, LLO, Virgo, KAGRA and LAO) at their nominal location and design sensitivity.

Credit: T. Bruel

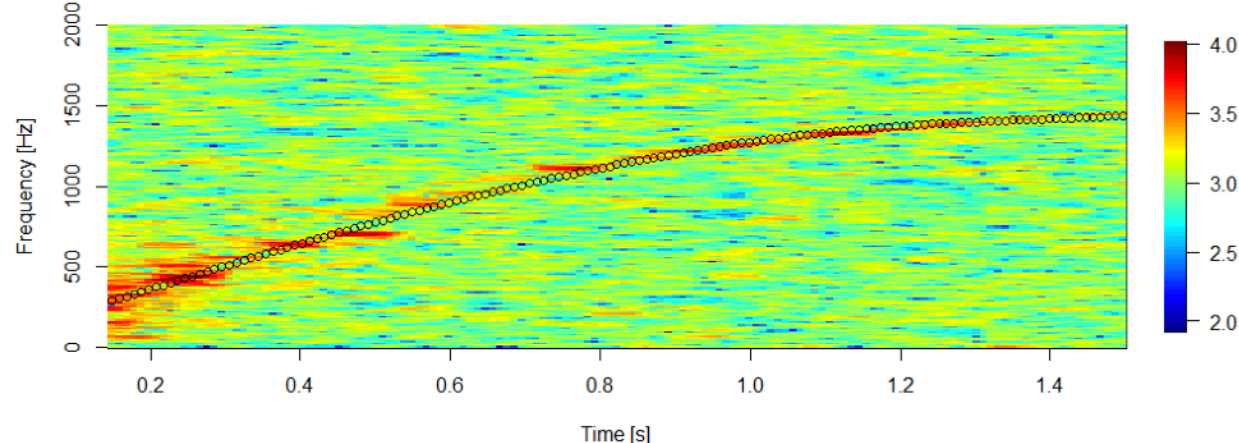
# Multi-detector coherent analysis

Coherent analysis of whitened data done following same method as in the X-pipeline  
(Sutton+ 2010)

Waveform: s20-LS220; Distance: 5 kpc; Detectors: LLO, LHO, Virgo, KAGRA



Signal track on spectrograms: LASSO fit (polynomial regression) on maxima



# Performance

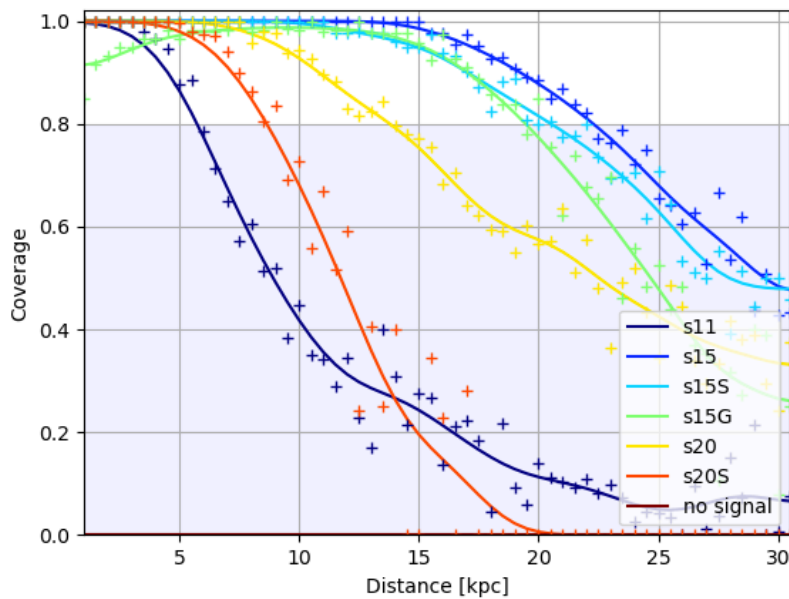
For a fixed source location we vary the distance.

**Waveform: s20-LS220**

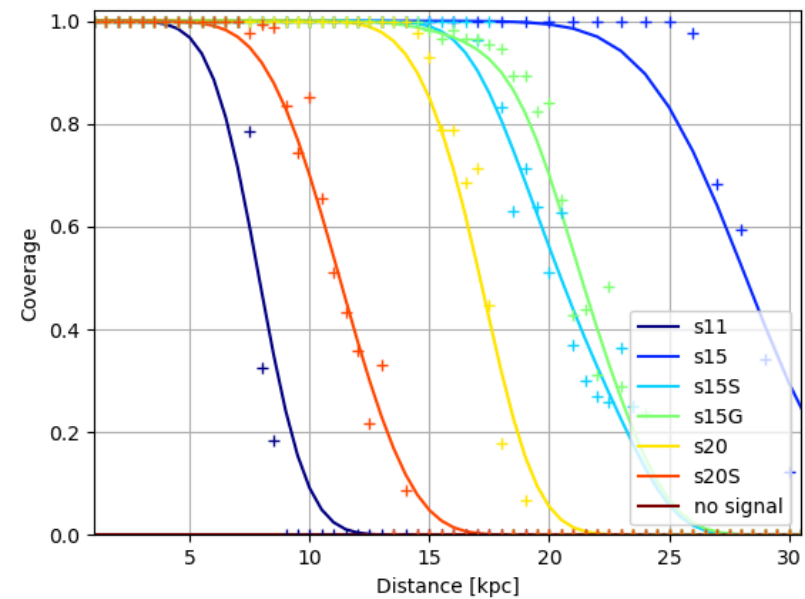
$$h = F^+(\alpha, \delta, \psi)h_+ + F^\times(\alpha, \delta, \psi)h_\times \quad \alpha = 8h \quad \delta = 60^\circ \quad \psi = 0^\circ$$

(strong antenna patterns  
 $F^+$  for the LIGO detectors)

$$\begin{matrix} F^+ & F^\times \\ \text{LHO} & -0.89 \quad 0.13 \end{matrix}$$



single-detector method



multi-detector method

Bruel+ 2021



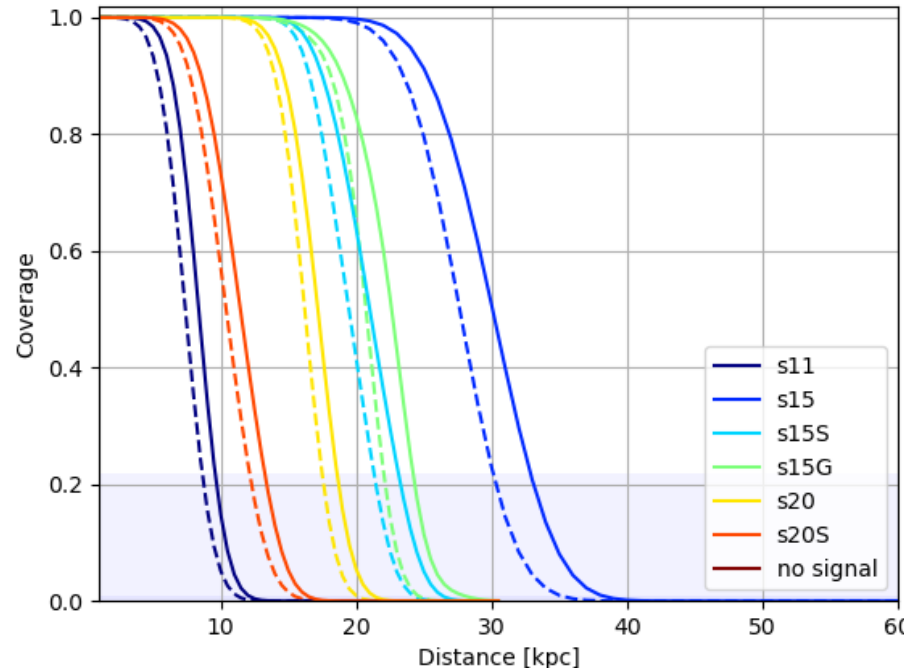
# Performance

For a fixed source location we vary the distance.

All waveforms

$$h = F^+(\alpha, \delta, \psi)h_+ + F^\times(\alpha, \delta, \psi)h_\times \quad \alpha = 8h \quad \delta = 60^\circ \quad \psi = 0^\circ$$

(strong antenna patterns  
 $F^+$  for the LIGO detectors)



Dashed lines: only two LIGO detectors

Solid lines: all five detectors (slight improvement  
despite Virgo, KAGRA and LAO not optimally aligned with source)

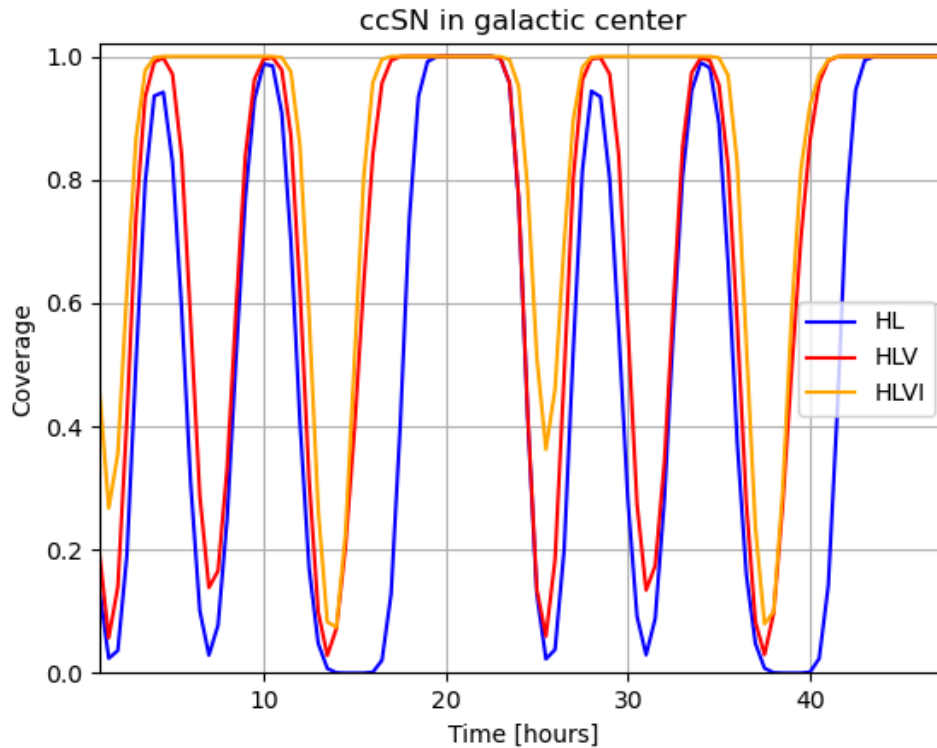
	$F^+$	$F^\times$
LHO	-0.89	0.13
LLO	0.81	-0.29
Virgo	0.24	0.56
KAG	-0.19	-0.05
LAO	-0.26	-0.35

multi-detector method

Bruel+ 2021



# Example: CCSN @ Galactic Center



Waveform: s20-LS220

Fixed sky position (galactic center)  
Time of arrival varies over 48h

3 networks: [HL, HLV, HLVI]

Mean coverage: [0.53, 0.70, 0.85]

The more detectors in the network, the higher the coverage and thus the chances of reconstructing the GW signal.

# Example: 3G detectors (2D waveform)

CCSN in nearby galaxies: average reconstruction probability.

Galaxies	Distance (kpc)	CE1 (phase 1)	CE1+CE2 (phase 1)	ET	CE1+CE2+ET (phase 1)
Large Magellanic Cloud	50	0.78	0.95	1	1
Small Magellanic Cloud	60.3	0.73	0.93	1	1
Ursa Minor Dwarf	68.4	0.68	0.91	0.99	1
Sculptor Dwarf	78.2	0.42	0.91	0.55	0.96
Draco Dwarf	79.1	0.55	0.87	0.68	0.96

Results for s20—LS220 waveform

Bruel+ 2021

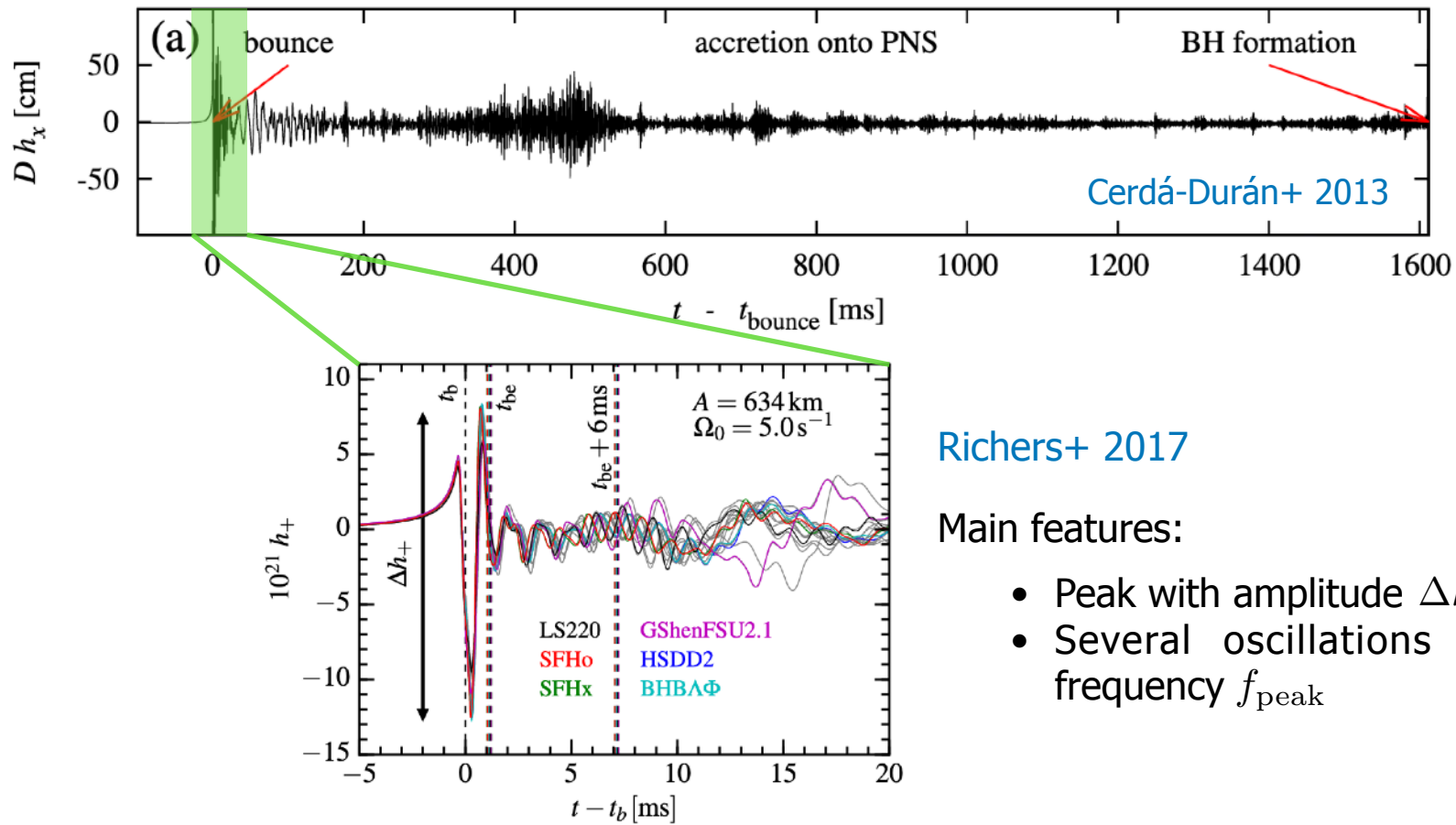
Must be repeated for all waveforms (ongoing)



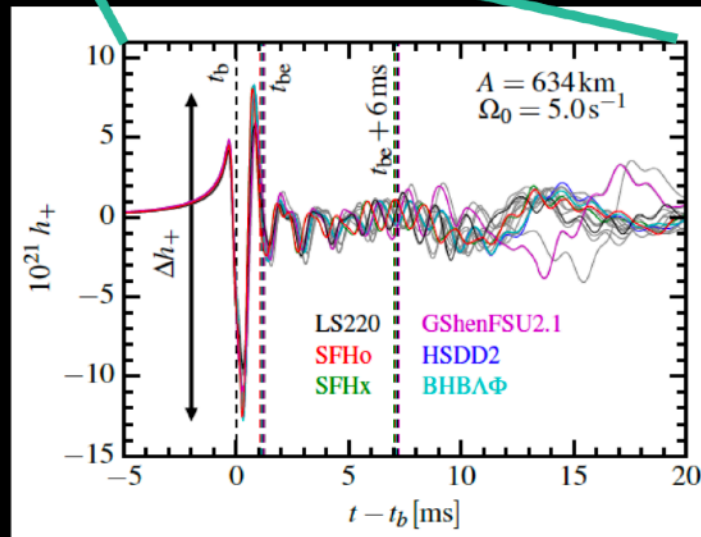
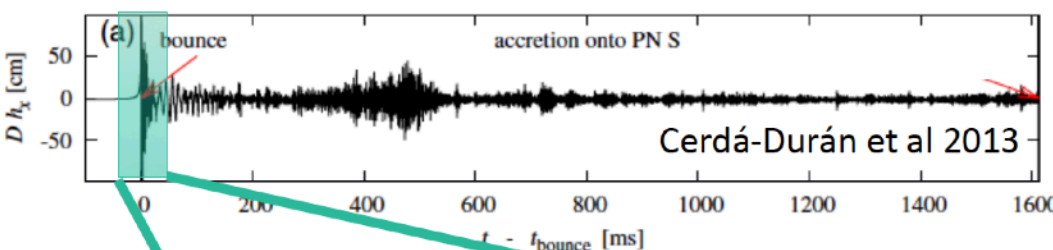
# Inference with rapidly rotating CCSN

The **peak GW emission at bounce** is related to the degree of **oblateness** of the core at bounce, which is related to the **rotation rate**.

Most comprehensive study of the bounce signal done by [Richers+ \(2017\)](#): over 1800 2D CCSN simulations (up to 10ms post-bounce). Only one GW polarization ( $h_+$ ) non-zero.



# Inference in rapidly rotating CCSN



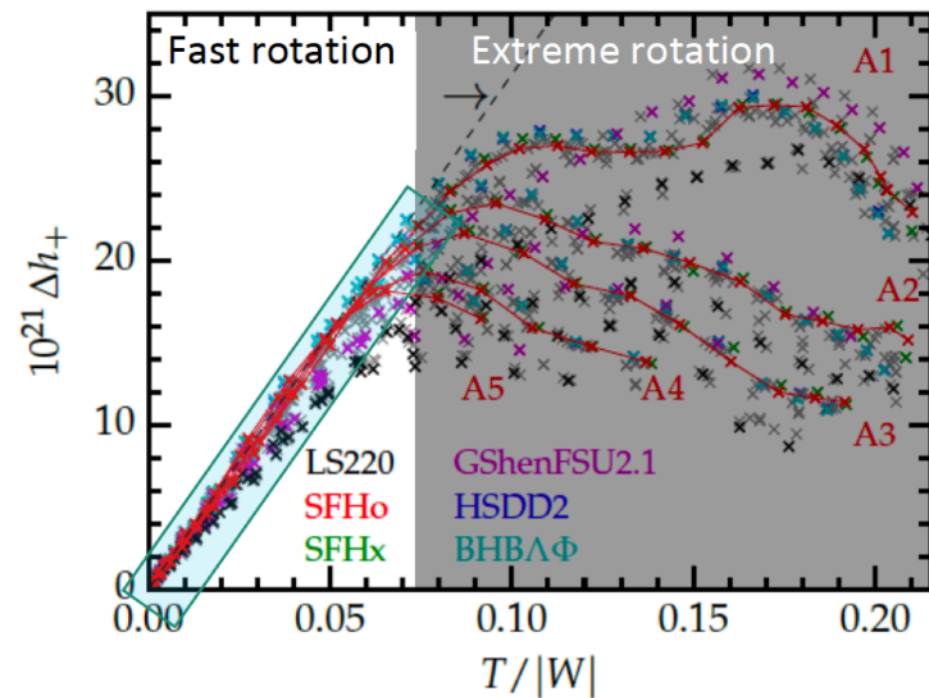
Richers et al 2017

- Only first few ms
- Only rotating models (zero for non-rotating): <1% SNe
- Main features:
  - Peak with amplitude  $\Delta h_+$
  - Several oscillations with frequency  $f_{\text{peak}}$
- Richers et al catalog:
  - 2D GR simulations
  - 1824 waveforms
  - 18 different EOS

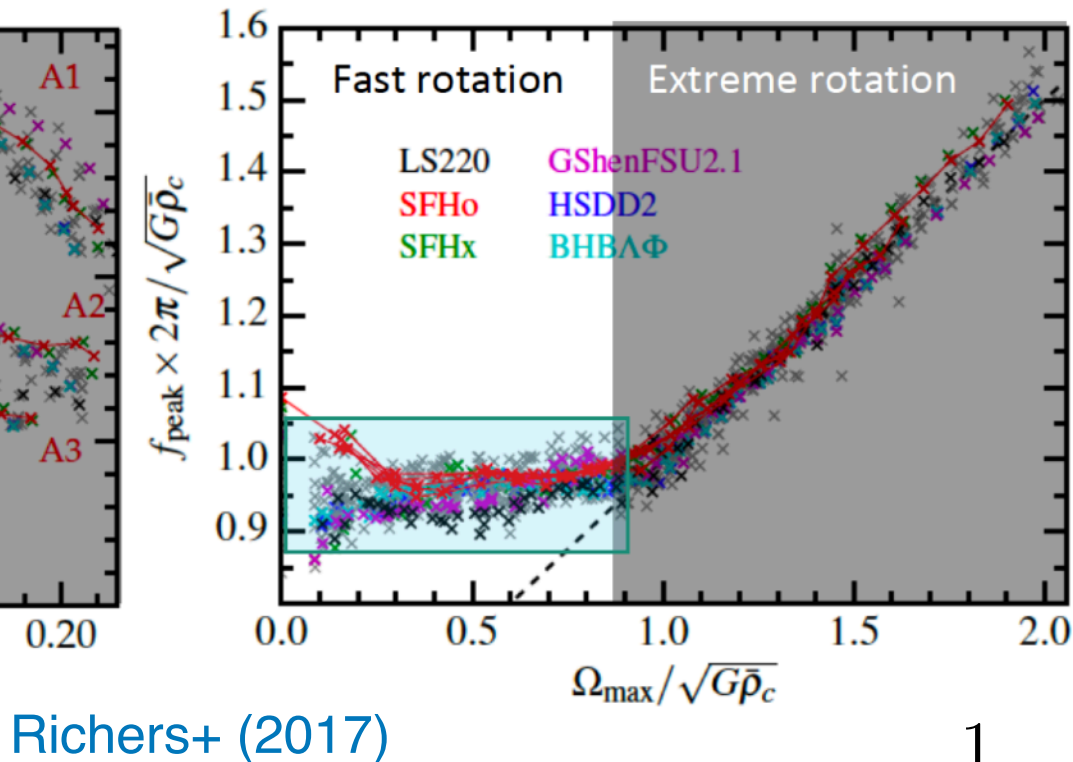
Q: What can we learn from performing PE on  $\Delta h_+$  and  $f_{\text{peak}}$  ?

A: We can estimate the **source parameters**:  $\rho_c$  and  $\frac{T}{|W|}$

# PE in rapidly rotating CCSN



$$\Delta h_+ \propto \frac{T}{|W|}$$



Richers+ (2017)

$$f_{\text{peak}} \propto \frac{1}{\sqrt{\rho_c}}$$

Q: What can we learn from performing PE on  $\Delta h_+$  and  $f_{\text{peak}}$  ?

A: We can estimate the **source parameters**:  $\rho_c$  and  $\frac{T}{|W|}$

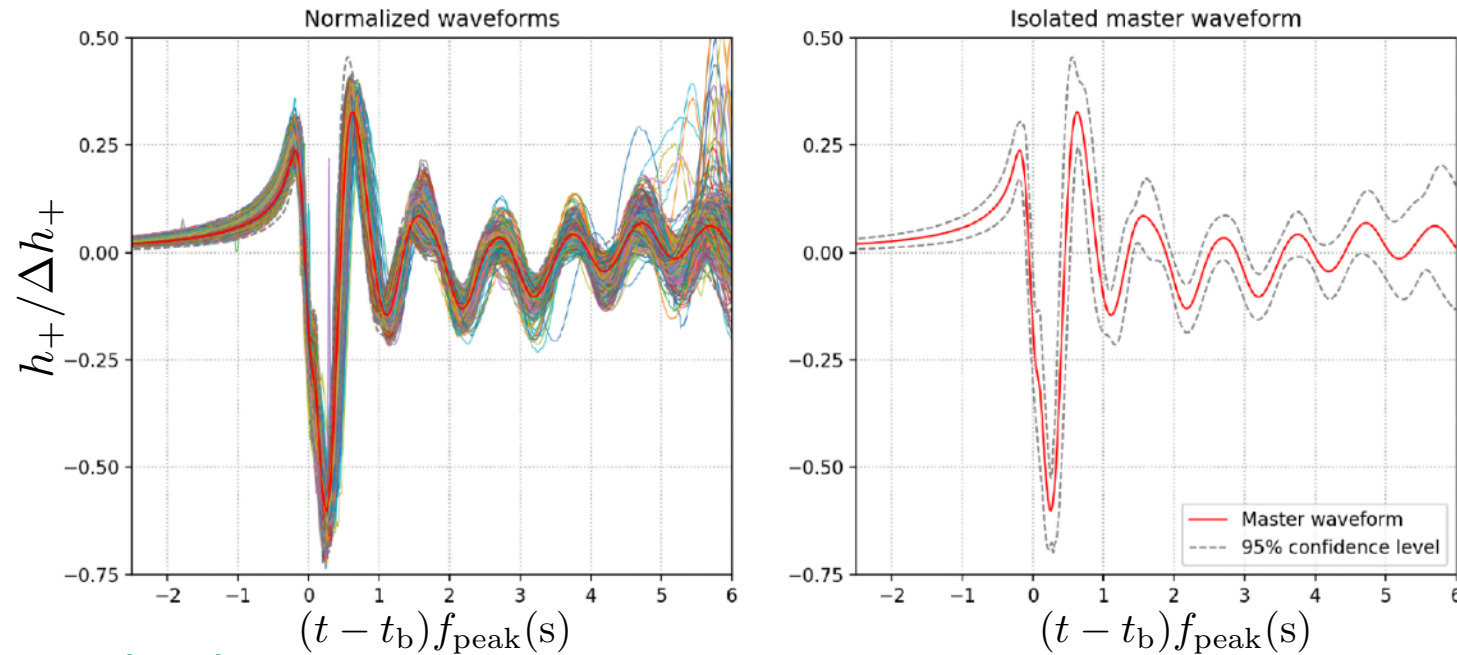
# PE in rapidly rotating CCSN - master waveform

Possible to describe a large fraction of the [Richers+ \(2017\)](#) waveforms in the early post-bounce phase in a simple form - **a master waveform template** - depending only on  $\Delta h_+$  and  $f_{\text{peak}}$

Include only models that (a) collapse, and (b)  $0 < \frac{T}{|W|} < 0.06$

Waveforms are: (a) aligned at time of bounce, (b) strain and time axes renormalized, (c) overlap late sinusoidal as much as possible.

Master waveform: average of **420 waveforms**.



[Pastor-Marcos+ \(2021\)](#)



# PE in rapidly rotating CCSN

Waveform model depends on **three parameters**:  $\theta = \{\Delta h_+, f_{\text{peak}}, \theta\}$

Perform **three series of injections** under different conditions (random values of parameters):

- Null injections with zero amplitude: only noise reference (no signal)
- Master waveform injections with  $f_{\text{peak}} \in [600, 1000]$  Hz and  $D \cdot \Delta h_+ \cdot \sin^2 \theta \in [0, 700]$  cm
- Random waveform injections among the 402 waveforms selected to build master template

Each series consists of 1000 injections on random Gaussian noise of a 3-detector HLV network at design sensitivity.

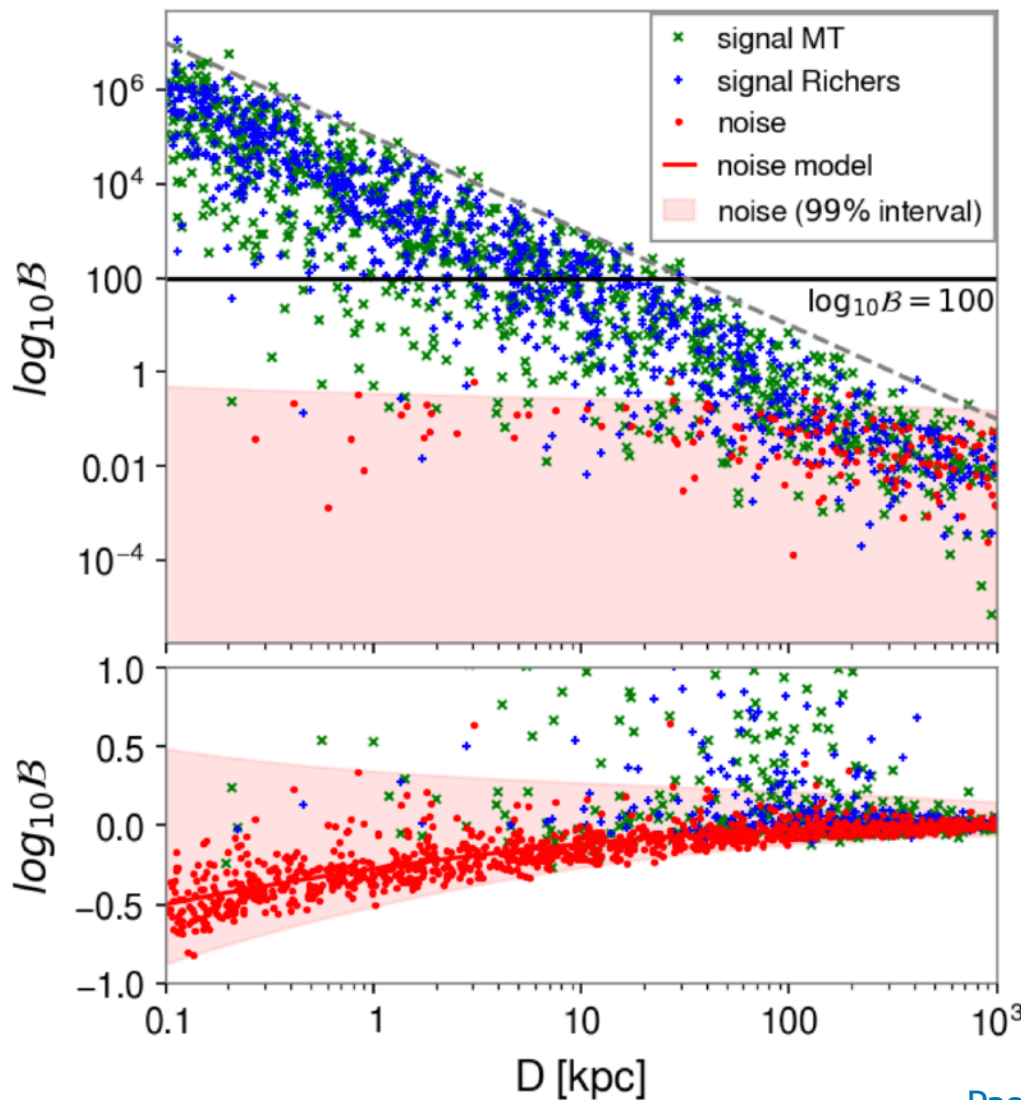
Injections performed at:

- Random sky location
- Random luminosity distance in 0.1-1000 kpc range
- Random inclination angle of rotation axis

For each injection, inference on (a)  $f_{\text{peak}}$  and (b)  $D \cdot \Delta h_+ \cdot \sin^2 \theta$  performed, assuming source location in the sky, source distance, and time of bounce known.



# PE in rapidly rotating CCSN - results



For signal injections:

$$\text{max of } \log_{10} \mathcal{B} \propto \frac{1}{D^2}$$

(upper limit for signals with maximum amplitude, optimal inclination and sky location.)

no influence of  $f_{\text{peak}}$  in  $\log_{10} \mathcal{B}$

For noise injections:  $\log_{10} \mathcal{B} \approx 0$

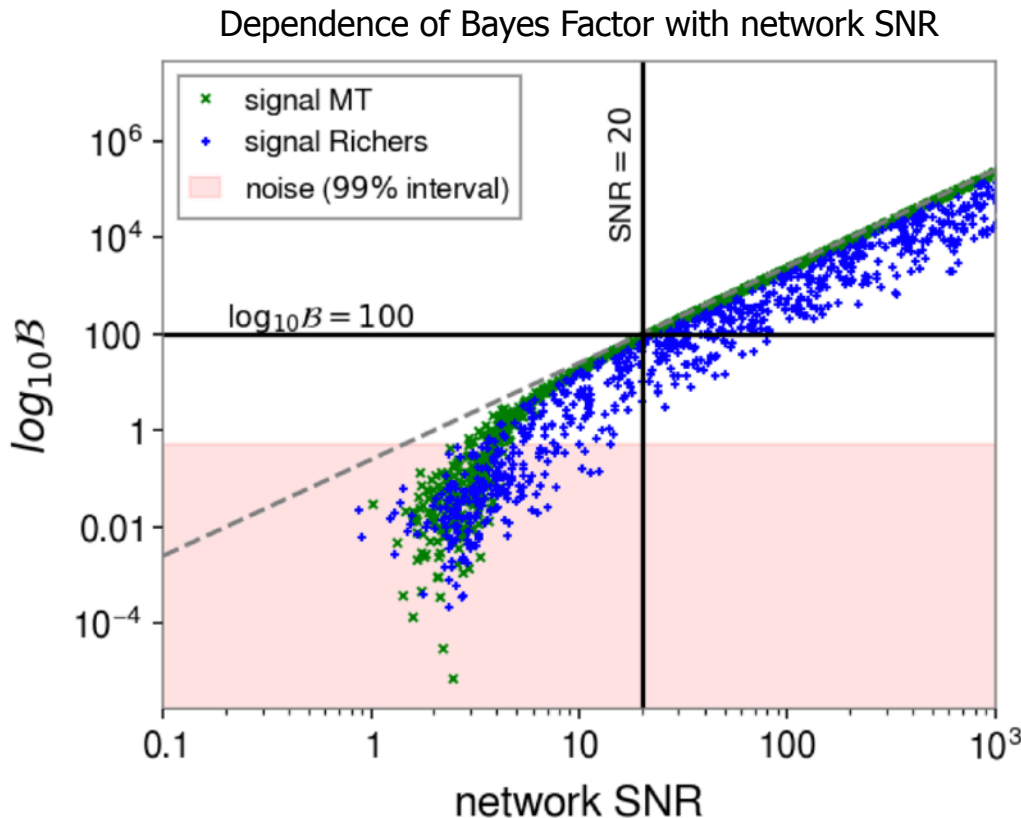
In general, signals with  $\log_{10} \mathcal{B} > 0.5$  are above the noise (99% CI)

Pastor-Marcos+ (2021)



# PE in rapidly rotating CCSN - results

cWB pipeline: over 50% of fast-rotating CCSN with SNR>20 are detectable in real detector noise conditions ([Szczepanczyk 2018](#)).



$\max \log_{10} \mathcal{B}$  proportional to network SNR squared (dashed line).

$\log_{10} \mathcal{B} > 100$  injections have  $\text{SNR} > 20$

43% of master waveform injections

46% of individual Richers waveform injections

Conservative estimate of the potential detectability of a fast-rotating CCSN signal based only on observed data.

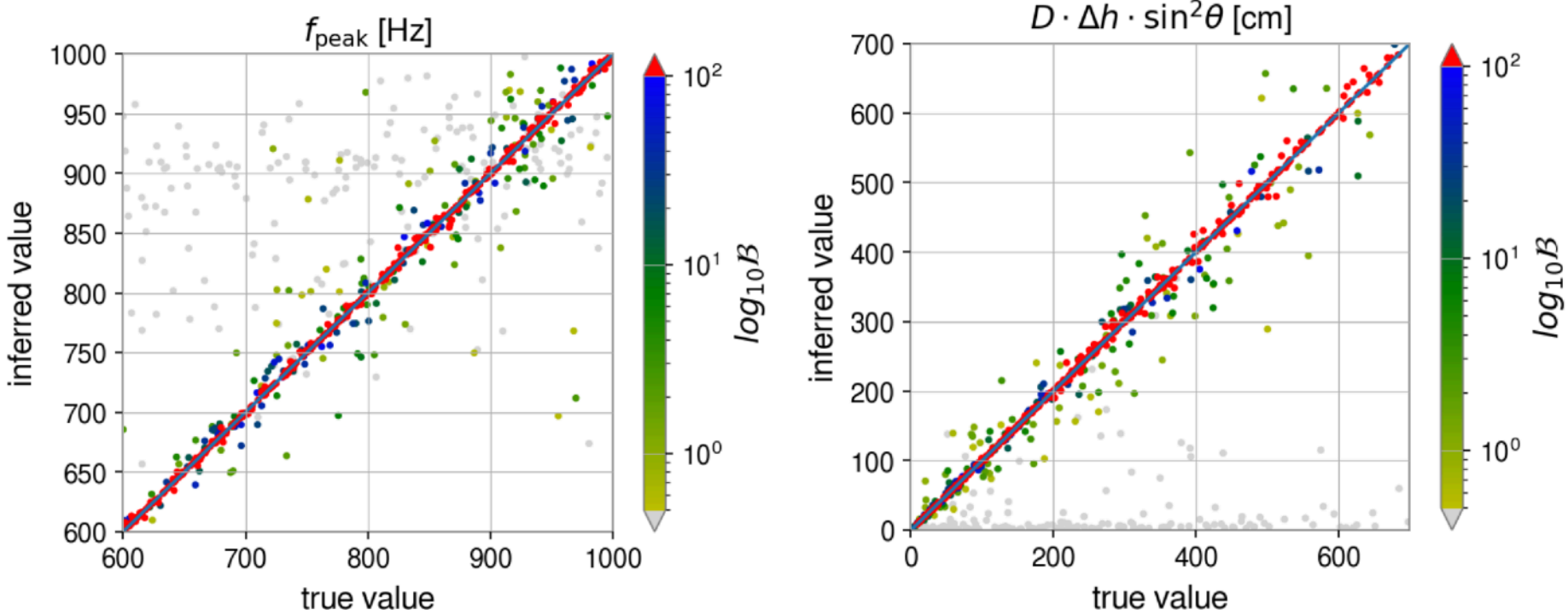
[Pastor-Marcos+ \(2021\)](#)



# PE in rapidly rotating CCSN - results

Master waveform injections.

Median of inferred posteriors vs true value of injected waveforms.



red  $\log_{10} \mathcal{B} > 100$  → Relative differences:

grey  $\log_{10} \mathcal{B} < 0.5$

<1.6%  $f_{\text{peak}}$

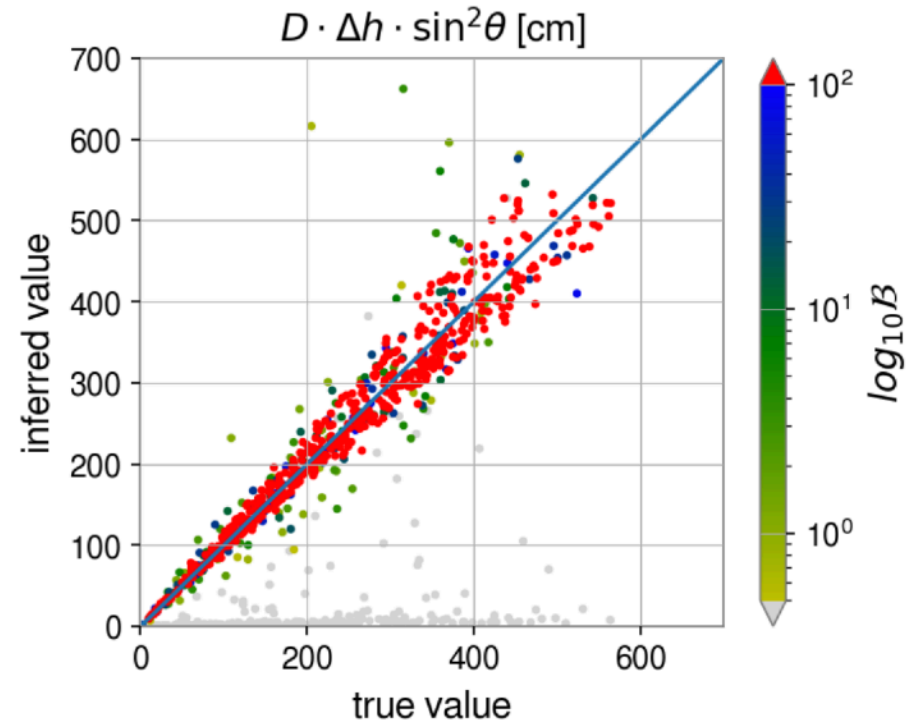
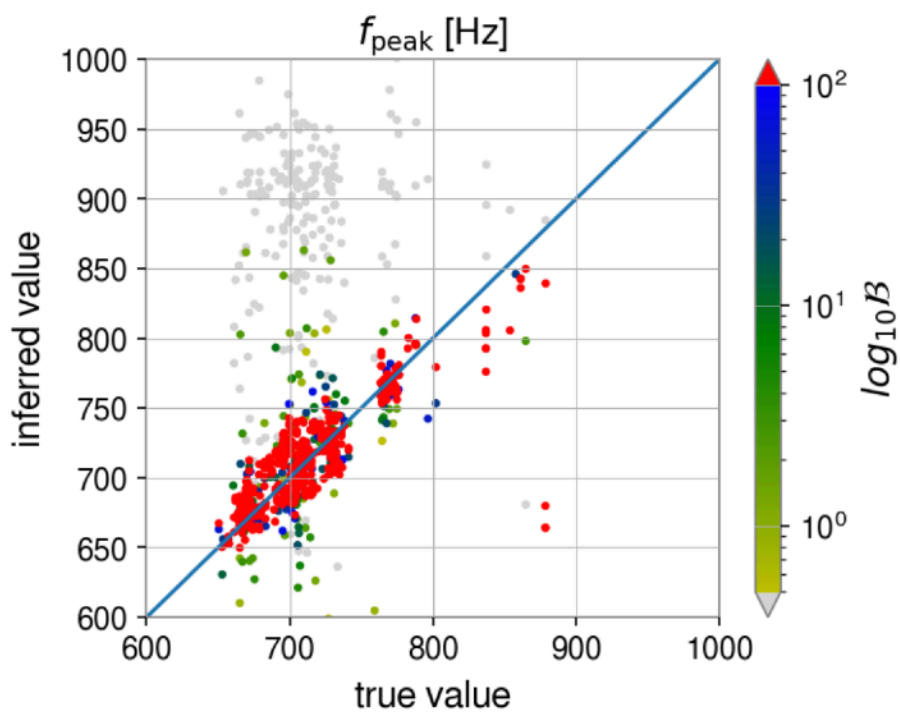
<10%  $D \cdot \Delta h_+ \cdot \sin^2 \theta$

Pastor-Marcos+ (2021)



# PE in rapidly rotating CCSN - results

Random waveform injections  
(master waveform does not perfectly match individual signals)



Larger dispersion of inferred values.

# Conclusions

- **Inference of PNS properties** using gravitational waveforms from CCSN may be **possible** in the future, following a successful detection.
- Illustrated with **two specific cases**:
  - Generic case (non-rotating CCSN, most common events)
  - Fast-rotating case (rare events)
- For generic CCSN, method based on the existence of quasi-universal relations between the frequency of oscillation of specific PNS modes and combinations of PNS parameters (mass and radius) and shock radius. **Asteroseismology of PNS**.
- For fast-rotating CCSN, a master waveform template can be built for the early bounce phase. Allows performing Bayesian inference on peak frequency and signal amplitude.
- Next steps:
  - Consider other PNS oscillation modes to disentangle properties (mass, radius).
  - Improve the mode analysis framework by considering 3D effects and rotation.
  - Employ different sets of waveforms for rapidly-rotating progenitors.

